Detection of water surface capillary wave by analysis of turning-point local signal data using a laser interferometer

Lieshan Zhang (张烈山), Xiaolin Zhang (张晓琳)*, and Wenyan Tang (唐文彦)

School of Electrical Engineering and Automation, Harbin Institute of Technology, Harbin 150001, China
**Corresponding author: zhangxiaolin@hit.edu.cn*

Received February 14, 2017; accepted April 14, 2017; posted online May 9, 2017

A laser interferometry technique is developed to detect water surface capillary waves caused by an impinging acoustic pressure field. The frequency and amplitude of the water surface capillary waves can be estimated from the local signal data at some special points of the phase modulated interference signal, which is called the turning points. Demodulation principles are proposed to explain this method. Experiments are conducted under conditions of different intensity and different frequency driving acoustic signals. The results show the local signal data analysis can effectively estimate the amplitude and frequency of water surface capillary waves.

OCIS codes: 120.3180, 120.7280, 010.7340.
doi: 10.3788/COL201715.071201.

A water surface capillary wave (WSCW) excited by underwater acoustic source is a transversely spread surface wave with an amplitude of several nanometers that carries some information about the underwater acoustic field. Interference detection of water surface micro amplitude waves is a new technique to extract the underwater acoustic field information[1–3]. Underwater acoustic signal detection is significant, especially in the field of submarine communications and underwater target recognition. The main applied technology of underwater acoustic field detection is still shipborne sonar detection technology[4], which needs a shipborne platform to host the main system and extends the acoustic sensor[5,6] into the water. Usually shipborne sonar lacks flexibility and concealment character.

Nowadays, more emphasis has been put on the remote sensing technology of underwater acoustic signals, such as the Doppler interference technology studied in this Letter. The laser interference method reported in Refs. [7,8], was used to determine the frequency of underwater acoustic signals by detecting the WSCWs that were excited by the underwater acoustic signals. We also did some work on the laser Doppler interference method to estimate the amplitude of water surface acoustic waves (WSAWs)[9], but these demodulation methods of coheret signal detection are only applicable for static analysis of a global signal. Blackmon *et al.*[10,11] used the laser Doppler vibrometer to directly detect the vibrations of the water surface to successfully obtain the acoustic frequency and sound pressure level of the underwater acoustic field. However, some large errors might be produced by this method due to the environmental disturbances (caused by wind or other factors). In this Letter, we used a simple laser homodyne system to detect the WSCW, and tried to analyze the local signal data to estimate the frequency and amplitude of WSCW. Then we proposed a demodulation method based on the analysis of local signal data at the turning points of interference signals. It is very difficult to obtain a stable interference signal in actual detections for natural water when using the laser Doppler interferometry technique, so a local signal data analysis method will be helpful in actual detection.

A simple Doppler homodyne interferometer was used to probe the water surface to detect the WSCW. There are some low frequency environmental perturbations on water surface. According to the principle of Doppler interferometery[7–13], when filtering out the DC component, the interference signal transduced by a photodetector can be described as[9]

$$U(t) = A_0 \cos[2kA_n \sin(\omega_n t + \varnothing_n) + 2kA_s \sin(\omega_s t + \varnothing_s) + \varphi_i], \tag{1}$$

where A_0 is the gain factor related to the optical amplitudes of two laser beams and the photoelectric conversion efficiency, and k is wave number of the coherent laser. The amplitude, the angular frequency, and the phase of environmental perturbations are denoted by A_n, ω_n, and $\varnothing_n$, respectively. Similarly, the amplitude, the angular frequency, and the phase of WSCW are denoted by A_s, ω_s, and $\varnothing_s$. The character t denotes time, and character φ_i is the initial phase caused by the optical path difference between the two arms of interferometer.

Usually the amplitude of WSCW is in the nanometer range, so it is completely submerged in the environmental perturbations. Due to the randomness of the environmental perturbations, complete and accurate phase demodulation of the laser interference signal is very difficult. Furthermore, the temporal phase change of the detection signal caused by WSCW is quite small, sometimes even smaller than a phase demodulation solution. As a result,

it is difficult to estimate the amplitude of the WSCW by signal phase demodulation.

When $\omega_n t + \varnothing_n = N\pi$, where N is an integer, the amplitude of the environmental perturbation wave reaches the maximum or minimum value. Because its frequency is quite small and its amplitude is very large, the frequency of WSCW is relatively large and its amplitude is extremely small. So, near these time spots, the phase change of the detection signal caused by the environmental perturbation wave is very slow, the high-frequency phase change caused by the WSCW can be clearly observed, and the phase modulation depth caused by WSAW reaches the deepest. We call these time spots the turning points of the detection signal, that is, at these time spots, environmental perturbation waves turn the vibrating direction. A simulation signal is depicted in Fig. 1, and the main parameter settings are as follows: the gain coefficient A_0 is 1, the laser operating wavelength is 632.8 nm, the amplitude of environmental perturbation wave A_n is set to 1 μm, the frequency of environmental perturbation wave ω_n is 20π rad/s, amplitude of WSCW A_s is set to 10 nm, its frequency ω_s is 4000π rad/s, and the initial phase φ_i is 0.35π. The red dotted line in Fig. 1 is the environmental perturbation wave. When the environmental perturbation reach the peaks and troughs (i.e., the turning points of simulation signal), the local high-frequency phase changes of simulation signal can be observed easily.

Near the signal's turning points, the phase change caused by environmental perturbation wave is so small that can be regarded as a constant value during a short time interval. In a certain short turning-point centered interval, if we regard $2kA_n \sin(\omega_n t + \varnothing_n) + \varphi_i$ as a constant value denoted by α, then the detection signal in Eq. (1) can be described as

$$U(t) = A_0 \cos\big[2kA_s \sin\,(\omega_s t + \varnothing_s) + \alpha\big]. \tag{2}$$

Using relevant formulas of the trigonometric and Bessel functions, denoting the phase modulation depth $2kA_s$ by x, and the whole phase of WSAW $(\omega_s t + \varnothing_s)$ by θ, Eq. (2) can be decomposed into

$$U(t) = A_0 \cos\alpha\left[J_0(x) + 2\sum_{m=1}^{\infty} J_{2m}(x)\cos 2m\theta\right] + 2A_0 \sin\alpha \sum_{m=0}^{\infty} J_{2m+1}(x)\cos\big[(2m+1)\theta\big]. \tag{3}$$

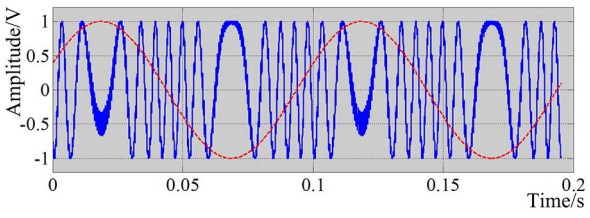

Fig. 1. (Color online) Simulation signal.

Since the amplitude of the WSCW is in the nanometer range, the order 2 and above Bessel function values of variable $2kA_s$ are closed to zero and far less than its first-order Bessel function value. As a result, we can neglect those high-frequency components in the signal in Eq. (3). So the interference detection signal near the turning points can be expressed as

$$U(t) \cong A_0 \cos\alpha J_0(x) + 2A_0 \sin\alpha J_1(x)\cos\theta. \tag{4}$$

When ignoring the DC component $A_0 \cos\alpha J_0(x)$, the local detection signal near the turning point can be considered to contain only one harmonic component with an amplitude of $2A_0 \sin\alpha J_1(x)$ and an angular frequency of ω_s. When $\alpha = 0.5\pi + N\pi$, the phase change of detection signal caused by WSCW reaches the most significance, and the intensity of the detection signal fluctuates around zero. As depicted in Fig. 2, we intercepted the local data signal centered at the first turning point of the simulation signal with a length of 512 points, the low-frequency trend component was stripped by using the empirical mode decomposition (EMD)[14] method, then a spectrum distribution of the local signal was achieved by a fast Fourier transform (FFT) algorithm, which is in good agreement with analysis above, that is to say, we can use the spectrum distribution of local signal near turning point to estimate the frequency of WSCW.

The influence of the gain coefficient A_0 can be eliminated by signal normalization. The amplitude of signal component ω_s near the turning point is $2 \sin\alpha J_1(x)$ at this time. At the turning point, when ignoring the high-frequency small fluctuations caused by WSCW, the amplitude of the DC component $\cos\alpha J_0(x)$ is numerically equal to the mean value of the local maximum value and minimum value near the turning point. Since A_s is extremely small and $J_0(x)$ is approximately equal to 1, the value of α can be deduced according to the signal intensity value at the turning point, and then the amplitude of ω_s component can be deduced according to the difference value between the local maximum value and minimum value at the turning point. If we denote the local maximum value by $A_{\max}$ and the local minimum value

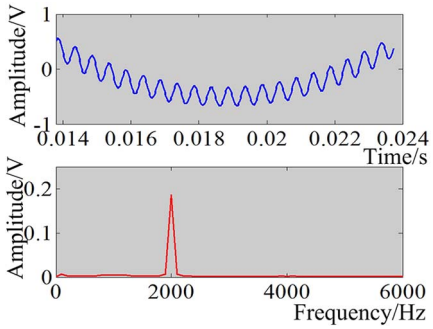

Fig. 2. First turning-point local signal data of the simulation signal and its Fourier spectrum.

by $A_{\min}$, then the first-order Bessel function value of modulation depth x is

$$J_1(x) = \frac{A_{\max} - A_{\min}}{4\sin\left[\arccos\left(0.5A_{\max} + 0.5A_{\min}\right)\right]}. \quad (5)$$

Then the amplitude of WSCW A_s can be calculated by the Bessel function tables according to the Eq. (5). For the simulation signal shown in Fig. 1, the local maximum value near the first turning point is −0.3277, and the local minimum value is −0.6703, then the calculated value of $J_1(x)$ is 0.0988 and A_s is 10.01 nm as computed by the Bessel function tables, which is in good agreement with the simulation designed value (10 nm). The calculated value of phase angle α is approximate 2.09 rad, which is in good agreement with the simulation designed value ($2kA_n + 0.35\pi = 6\pi + 2.10$ rad).

Intuitively, high-frequency fluctuations can be observed more significantly near the turning point of the detection signal. According to the time-domain distribution of the simulation signal shown in Fig. 1, the turning points of the detection signal appear at the crest or trough of the environmental perturbation waves. After filtering out the high-frequency components, the processed signal, which is called the base signal, implies information of the environmental perturbation waves. Calculating the local extreme points of the base signal, and we defined these extreme points as the characteristic points, we can conclude that: (1) the phase modulation effect of WSCW in the turning-point local signal plays the dominant role, which results in the presence of a high-frequency component in frequency domain of the local signal; (2) the turning points are located at the characteristic points of the base signal, whose signal intensity usually lower than the adjacent same-polarity characteristic points; (3) there are relatively larger time intervals between the turning points and other characteristic points; (4) at the turning points, the base signal has a large curvature radius.

The turning points can be extracted easily from the detection signal according to the above four tips. Due to the randomness of nature water surface waves, the turning-point distribution of an actual detection signal is not as regular as the simulation signal, but its distribution characteristics still conform to the four tips above. To eliminate the effect of signal gain coefficient A_0, the signal needs to be normalized. Usually we extract the envelope function of the base signal, and then divide every point intensity value of the original signal by the corresponding envelope function value.

We set up an experimental system shown in Fig. 3, which can be divided into three functional modules: (1) the WSCW excitation module; (2) the laser Doppler interference detection system; (3) the detection signal acquisition and processing module. The WSCW excitation module consists of a signal generator, a power amplifier, and an underwater eletroacoustic transducer. A standard sinusoidal voltage signal sent by a signal generator was applied to drive an underwater eletroacoustic transducer

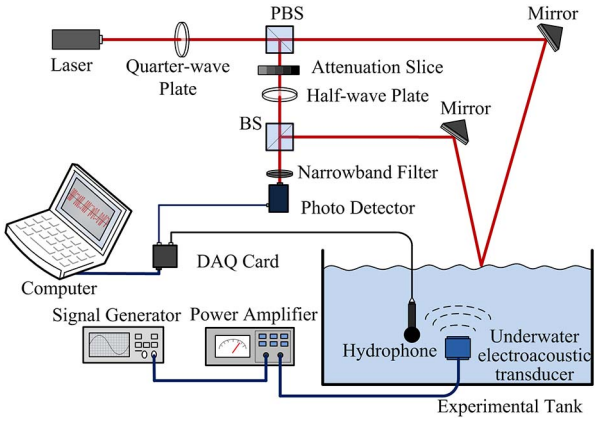

Fig. 3. Schematic diagram of experimental system.

to produce a sound field and excite the WSCW. The underwater eletroacoustic transducer, which was positioned in water with a depth about 0.5 m, can generate a highly directional acoustic signal, i.e., this module could simulate a far-field plane acoustic wave, which is consistent with the actual situation. A standard hydrophone was also installed in the tank to monitor the acoustic radiation intensity of the eletroacoustic transducer. The measuring principle of the laser Doppler interference system in Fig. 3 is very simple, we will not describe it any further in this Letter.

The Doppler interference detection system was used to detect the WSAWs. Experiments on steady frequency WSCWs were conducted, and the 2 kHz WSCW detection experiments were taken as examples to demonstrate that the local data analysis method could evaluate the frequency and amplitude of WSCW. A 2 kHz standard sinusoidal signal sent by the signal generator was amplified to drive the underwater eletroacoustic transducer. Since the characteristic acoustic impedance of air is much less than that of water, the air-water interface presents an impedance mismatch. The water surface vibrated in response to the impinging acoustic field, as a result, WSCW was produced. The voltage of the driving signal remained steady (the peak-to-peak value of driving signal voltage is 1 V in the experiment), and the laser detection signal of 2 kHz WSCW acquired by data acquisition (DAQ) card is shown in Fig. 4. In the frequency domain, dense spectral lines appear around 2 kHz, and the frequency band consisting of these spectral lines is centered at the frequency of 2 kHz. In Ref. [8], frequency of WSCW was determined according to this characteristic.

After filtering out the high-frequency components of the detection signal, we got the base signal and calculated its characteristic points. After that, the turning points were selected according to the time interval between the characteristic points and the curvature of the base signal at the characteristic points. The turning points of the detection signal and envelopes of the base signal are shown in Fig. 5.

A short local signal with a length of 720 points centered at the first turning point was intercepted to realize further

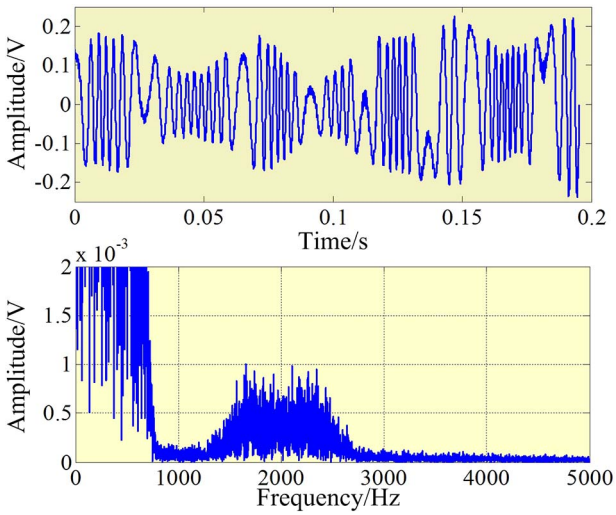

Fig. 4. Interference detection signal of 2 kHz WSCW.

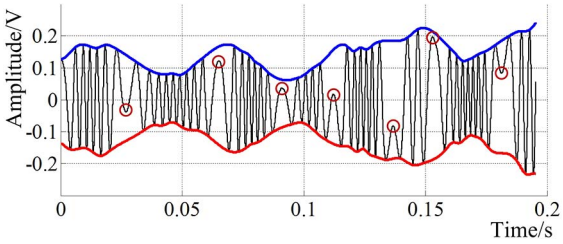

Fig. 5. Distribution of turning points (in circles) and envelopes of the base signal.

analysis. We extracted the high-frequency component from this local signal by using EMD. The waveform and spectrum distribution of the high-frequency intrinsic mode function (IMF)[14] component are shown in Fig. 6. According to the spectrum distribution, the dominant component is at the frequency of about 2 kHz, and this coincides with the theoretical analysis in the previous paragraphs.

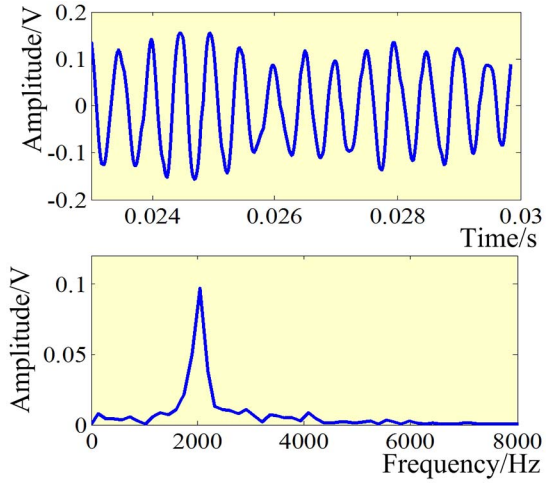

Fig. 6. Time domain and frequency domain distribution of the first turning point local signal.

The spline interpolation method was used to fit the characteristic points to extract the upper and lower envelopes of the base signal as depicted in Fig. 5. It can be observed from the figure that the upper and lower envelopes are roughly symmetrical, this amplitude modulation is generated by the shaking of detection light, which is caused by the large scale and random environmental perturbations on the water surface. After signal normalization, the basic frequency of each local signal was determined by EMD and Fourier analysis, the local extreme values $A_{\max}$ and $A_{\min}$ were extracted, the phase difference α at the turning point and the amplitude A_s of WSAW were estimated according to Eq. (5). The processing results of local signals at the turning points are given in Table 1. Actually, the calculated amplitude A_s is not equal to the out-of-plane displacement of water surface. The out-of-plane displacement equals to $A_s\cos(\vartheta_i)$, where ϑ_i is the incident angle of the detection light. The incident angle in the experiment is so small (about 15°) that it can be neglected.

According to Table 1, the basic frequencies f_b of the seven turning-point local signals are the same value of 1991.1 Hz, which coincides with the set value of the driving signal 2000 Hz, and indicates that the local data processing method can measure the frequency of the WSCW. The errors are mainly caused by the frequency resolution of FFT method, i.e., they depend on the length of local signal and the sampling rate of the DAQ card, the model of DAQ card we used is NI 9232 (its sampling rate is 102.4 kS/s, and the resolution is 24 bits).

It can be inferred that the basic phase α at each turning-point is variable because of the randomness of the water surface perturbations. The basic phase at the No. 6 turning point is much smaller, which results waveform distortions of the high-frequency component. The signal intensity value of normalized base signal at the No. 6 turning-point is very close to 1. So, when superposed with a high-frequency component at the No. 6 turning point, the waveform distortion takes place. Ignoring the stability of output power of the eletroacoustic transducer, the amplitude of WSCW could be estimated at 5.85 nm by using

Table 1. Processing Results of the Local Signals

No.	f_b/Hz	$A_{\max}$/V	$A_{\min}$/V	α/rad	A_s/nm
1	1991.1	−0.1571	−0.3660	1.8354	5.5
2	1991.1	0.8452	0.7039	0.6848	5.6
3	1991.1	0.6106	0.3912	1.0462	6.4
4	1991.1	0.2061	−0.0329	1.4841	6.0
5	1991.1	−0.3021	−0.5081	1.9879	5.7
6	1991.1	1.0002	0.8671	0.3663	9.4
7	1991.1	0.5434	0.3267	1.1207	6.1

the method present in the Ref. [9]. Despite the large calculation error of amplitude A_s at the No. 6 turning-point, the amplitude of WSCW can be effectively estimated by this method.

Experiments under conditions of different intensity driving acoustic signals were also conducted. We set 9 different peak-to-peak voltage driving signals from 1 to 5 V, to excite different amplitude WSCWs. For each driving signal, we used the local data processing method mentioned above to estimate the amplitudes of WSCW at each turning point, and took their mean value as the final measurement result. The amplitude measurement results of the WSCWs under conditions of different driving signals are depicted in Fig. 7(a). The figure shows that the amplitude increases, while the voltage of the driving signal increases, which demonstrates the efficiency of the local data processing method in estimating the amplitude of the WSCW. When the voltage of the driving signal was set to the value from 1 to 3 V, the amplitude of WSCW increased linearly. However, due to the response characteristics of the underwater eletroacoustic transducer, when the voltage of driving signal was larger than 3 V, the amplitude of WSCW did not significantly increase. This behavior is in accordance with the acoustic monitoring results of the hydrophone. We can qualitatively observe the change in underwater sound pressure through the amplitude of the 2 kHz component in the hydrophone-generated electrical signal, as shown in Fig. 7(b).

Environmental perturbation, like the thermal capillary wave, are the main factor of so-called surface roughness, which make the detection light scatter. As long as the intensity of coherent component in scattering light is evidently larger than that of incoherent components, we can acquire a good interferometer signal. According to the theories of electromagnetic scattering, we infer that this method can cope with a millimeter-range environmental perturbation.

A sweep frequency WSCW was excited by a sweep acoustic signal. The starting frequency was 1 kHz, cutoff frequency was 4 kHz, and the frequency change period was 1 s; therefore, the frequency rate of change was 3 kHz/s. The WSCW detection signal with a length of 1 s was acquired, and there were 34 turning-points extracted from the detection signal. Next, the short-time

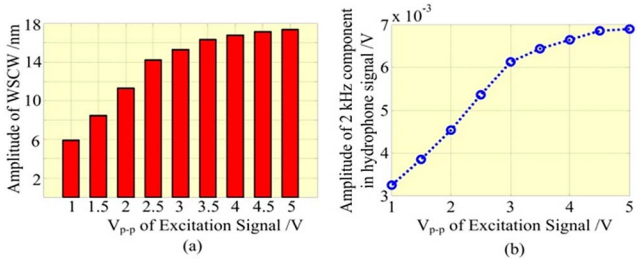

Fig. 7. Amplitudes of (a) WSCWs and (b) hydrophone monitoring results under conditions of different driving signal.

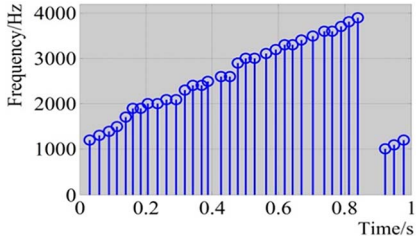

Fig. 8. Basic frequencies of the turning-point local signals.

local signals centered at each turning point were decomposed by EMD. The dominant frequency was obtained by Fourier analysis of the extracted high-frequency IMF component. The dominant frequency estimated results from 34 turning-point local signals are depicted in Fig. 8. It can be seen from Fig. 8 that the frequency of the WSCW changes from low to high in the observation time interval. When the frequency increases to about 4 kHz (at the time of about 0.85 s), the frequency of the WSCW, which coincides with the sweep signal characteristics we set, decreases instantly to about 1 kHz. This proves that the turning-point local data processing method can track the frequency change of the WSCW. The foremost 31 data points in Fig. 8 are fitted to a line and the calculated frequency rate of change (i.e., the slope of the fit line) of WSCW is 3.06 kHz/s, which is almost the same with the value we set.

In conclusion, a laser interferometry system is developed to detect WSCW, and a method based on the turning-point local signal data analysis is proposed to estimate the amplitude and frequency of the WSCW. According to the theoretical and experimental analysis, we can conclude that: (1) high-frequency phase changes at turning points caused by WSCW can be obviously observed in the detection signal, and the phase modulation effect of the WSCW plays a dominant role in the turning- point short local signals; (2) experiments for 2 kHz WSCWs excited by different intensity driving signals show that the turning-point local signal analysis method can effectively estimate the amplitude of WSCW and track its changes; (3) experiments for 2 kHz and sweep frequency WSCWs show that the turning-point local signal analysis method can also estimate the frequency of WSCW and track the frequency changes.

This work was supported by the National Natural Science Foundation of China (No. 61108073) and the Shanghai Aerospace Science Technology Foundation (No. 2015029).

References

1. I. B. Esipov and S. Y. Pashin, Sov. Phys. Acoust. **36**, 433 (1990).
2. J. H. Churnside, H. E. Bravo, K. A. Naugolnykh, and I. M. Fuks, Acoust. Phys. **54**, 204 (2008).
3. D. Farrant, J. Burke, L. Dickinson, P. Fairman, and J. Wendoloski, in *Proceedings of OCEANS'10 IEEE Sydney* (2010).
4. A. Mours, C. Ioana, J. I. Mars, N. F. Josso, and Y. Doisy, J. Acoust. Soc. Am. **140**, 1771 (2016).

5. Z. Wang, Y. Hu, Z. Meng, and M. Ni, Chin. Opt. Lett. **6**, 381 (2008).
6. N. Beverini, S. Firpi, P. Guerrini, E. Maccioni, A. Maguer, M. Morganti, F. Stefani, and C. Trono, Proc. SPIE **7994**, 79941D (2011).
7. H.-P. Duan, W.-Y. Tang, L.-H. Liu, and X.-L. Zhang, J. Optoelectron. Laser **20**, 1189 (2009).
8. X.-L. Zhang, W.-Y. Tang, and H.-Y. Sun, Opt. Prec. Eng. **18**, 809 (2010).
9. L. Zhang, X. Zhang, and W. Tang, Chin. Opt. Lett. **13**, 091202 (2015).
10. F. A. Blackmon and L. T. Antonelli, IEEE J. Oceanic Eng. **31**, 179 (2006).
11. L. Antonelli and B. Fletcher, in *Proceedings of Oceans Conference Record* (IEEE, 2002), p. 1949.
12. W. Sun, J. Liu, H. Gui, A. Lu, H. Wang, and Y. Lu, Chin. Opt. Lett. **14**, 021201(2016).
13. Y. Zhu, L. Wang, M. Zhang, S. Lu, K. Yang, and C. Hu, Chin. Opt. Lett. **14**, 061201 (2016).
14. M. Kedadouche, M. Thomas, and A. Tahan, Mech. Syst. Signal Process. **81**, 88 (2016).